

Article

# Effect of Heat Wave Conditions on Aerosol Optical Properties Derived from Satellite and Ground-Based Remote Sensing over Poland

Iwona S. Stachlewska <sup>1,\*</sup> , Olga Zawadzka <sup>1</sup> and Ronny Engelmann <sup>2</sup>

<sup>1</sup> Faculty of Physics, Institute of Geophysics, University of Warsaw, 02-093 Warsaw, Poland; zawadzka@igf.fuw.edu.pl

<sup>2</sup> Leibniz Institute for Tropospheric Research, 04318 Leipzig, Germany; ronny@tropos.de

\* Correspondence: iwona.stachlewska@igf.fuw.edu.pl

Received: 8 October 2017; Accepted: 20 November 2017; Published: 22 November 2017

**Abstract:** During an exceptionally warm September in 2016, unique and stable weather conditions contributed to a heat wave over Poland, allowing for observations of aerosol optical properties, using a variety of ground-based and satellite remote sensors. The data set collected during 11–16 September 2016 was analysed in terms of aerosol transport (HYbrid Single-Particle Lagrangian Integrated Trajectory model (HYSPLIT)), aerosol load model simulations (Copernicus Atmosphere Monitoring Service (CAMS), Navy Aerosol Analysis and Prediction System (NAAPS), Global Environmental Multiscale–Air Quality (GEM-AQ), columnar aerosol load measured at ground level (Aerosol Robotic NETwork (AERONET), Polish Aerosol Research Network (PolandAOD)) and from satellites (Spinning Enhanced Visible and Infrared Imager (SEVIRI), Moderate Resolution Imaging Spectroradiometer (MODIS)), as well as with 24/7 PollyXT Raman Lidar observations at the European Aerosol Research Lidar Network (EARLINET) site in Warsaw. Analyses revealed a single day of a relatively clean background aerosol related to an Arctic air-mass inflow, surrounded by a few days with a well increased aerosol load of differing origin: pollution transported from Germany and biomass burning from Ukraine. Such conditions proved excellent to test developed-in-house algorithms designed for near real-time aerosol optical depth (AOD) derivation from the SEVIRI sensor. The SEVIRI AOD maps derived over the territory of Poland, with an exceptionally high resolution (every 15 min;  $5.5 \times 5.5 \text{ km}^2$ ), revealed on an hourly scale, very low aerosol variability due to heat wave conditions. Comparisons of SEVIRI with NAAPS and CAMS AOD maps show strong qualitative similarities; however, NAAPS underestimates AOD and CAMS tends to underestimate it on relatively clean days ( $<0.2$ ), and overestimate it for a high aerosol load ( $>0.4$ ). A slight underestimation of the SEVIRI AOD is reported for pixel-to-column comparisons with AODs of several radiometers (AERONET, PolandAOD) and Lidar (EARLINET) with high correlation coefficients ( $r^2$  of 0.8–0.91) and low root-mean-square error (RMSE of 0.03–0.05). A heat wave driven increase of the boundary layer height of 10% is accompanied with the AOD increase of 8–12% for an urban site dominated by anthropogenic pollution. Contrary trend, with an AOD decrease of around 4% for a rural site dominated by a long-range transported biomass burning aerosol is reported. There is a positive feedback of heat wave conditions on local and transported pollution and an extenuating effect on transported biomass burning aerosol. The daytime mean SEVIRI PM<sub>2.5</sub> converted from the SEVIRI AODs at a pixel representative for Warsaw is in agreement with the daily mean PM<sub>2.5</sub> surface measurements, whereby SEVIRI PM<sub>2.5</sub> and Lidar-derived Ångström exponent are anti-correlated.

**Keywords:** aerosol optical depth; Raman Lidar; SEVIRI AOD to PM<sub>2.5</sub> conversion; heat wave

## 1. Introduction

There is a recognized potential for applications at a regional-scale of such controversial measures as injections of sulphate aerosols into the stratosphere, with an aim at offsetting the impacts of heat waves [1]. Indeed, heat waves are an important factor in climate research [2,3]. In Central Europe they form during a stagnating, stationary, high-pressure weather situation, when a high-pressure system, slowly subsiding in the upper atmosphere traps the heat near the ground [4]. The high temperatures during heat wave events can favor the development of intense local forest fires. These can cause an increase in the aerosol amount over the areas affected by the heat wave and also have a large impact on aerosol properties normally observed [5]. Thus, large changes of radiative fluxes at surface, at in the free troposphere as well as at top-of-atmosphere (TOA) can be expected [6]. However, the mutual effects (if any) of long-range transported forest, peatland or grass fire's aerosols on heat waves have not been undertaken thus far.

Depending on their type, the suspended aerosols directly and indirectly affect the local, regional and global temperature, causing a cooling or warming effect at the surface, at the altitude of the aerosol layer occurrence, and at top-of-atmosphere [7]. Wind speed, height of the boundary layer top and temperature profiles have significant impact on the vertical distribution of the aerosol optical and microphysical properties in the lower troposphere [8–10]. Concentrations of air pollutants are strongly regulated by the planetary boundary layer, and better understanding of the evolution of the height of the boundary layer top is important for the regulation of air pollutants in large cities [11]. However, the intuitive relation of the boundary layer height to the heat wave conditions needs investigation.

Both ozone and wild fire aerosols effects on the particulate matter (PM) air quality are expected to be significant and will become an increasing consideration [12]. Low turbulence diffusion and PBL height are also important meteorological factors affecting air pollution episodes, as is evident from their correlation with near-surface PM<sub>2.5</sub>, either on a regional or diurnal basis [13]. Despite considerable improvements in the past decades, Europe is still advancing towards achieving levels of air quality that do not pose unacceptable hazards to humans and the environment [14]. During extreme weather events such as heat waves, the air quality issues become of increased importance. Interaction between high levels of air pollution and high temperature ( $\geq 30$  °C) are reported as statistically significant ( $p < 0.05$ ) for sulphur dioxide, and as suggested ( $p < 0.2$ ), for ozone and smoke [15], and therefore under such conditions, inhabitants of urban areas can experience significant health problems due to air pollution.

Already a decade ago, researchers indicated that future heat waves will become more intense, more frequent and longer lasting due to the relationship between global warming and occurrence of regional heat waves [2,3]. Moreover, many prevalent human diseases are linked to such climate fluctuations [16]. A significant proportion of the deaths being attributed to the hot summer weather may have been caused solely by air pollution [17]. However, a recently reported interaction between high temperatures and wild fire air pollution needs to be considered in health risk assessments, particularly because the two often occur together [18].

Weather conditions forming heat wave events can also contribute to the formation of multiple layers that can be attributed to air masses of different origins: local and advection driven [19–21]. Aerosol layers can be simultaneously observed only by means of the quasi-continuous, height-resolved active ground-based, airborne or satellite remote sensors such as Lidars. For multi-layered structures, a correct interpretation of the aerosol type from the passive remote sensors, such as photometers and radiometers that provide information on the spectrally dependent columnar aerosol optical depth, is hindered. However, both passive and active remote observations from ground-based and satellite platforms can strongly contribute to air pollution research.

The European Space Agency (ESA) funded project, entitled satellite based Monitoring Initiative for Regional Air quality (SAMIRA), aims at improving regional and local air quality monitoring through synergistic use of data from present and upcoming satellite missions, traditionally used in situ air quality monitoring networks, as well as output from chemical transport models. One of the

targeted areas is Poland, a country confronted with pressing air quality problems such as smog alerts in industrial areas of Upper Silesia [22,23], frequent biomass burning transport from Ukraine and Belarus [24,25] and Northern America [19–21], as well as mineral dust intrusions [19,24]. These goals can be addressed among others, by a challenging topic of accurate daytime and night-time Aerosol Optical Depth (AOD) estimation from existing sensors on board satellites. The challenge here is not solely appropriate cloud mask filtering [26,27]. The satellite retrieval of aerosol properties over land is a difficult task, mainly due to estimation of the surface reflectance (in terms of its high temporal variability and spatial inhomogeneity) and the anisotropic bi-directional reflectance of land surfaces (inducing higher uncertainties of retrieved parameters) [28–30]. However, the satellite-derived AODs are recognized as an important predictor of ground-level particulate matter (PM), which empowers the air pollution research [31,32].

In this paper we discuss a variety of remote sensing observations, conducted during the heat wave event caused by the large anticyclonic high pressure system, spreading extensively over Central Europe, which trapped the warm air brought from Africa over Spain to Western, Central and Eastern Europe. During the second week of September 2016, in some countries, the heat wave caused extraordinary temperature records, e.g., in the United Kingdom, the highest September temperature of +34.4 °C (in shadow) since 1911 was recorded; in Spain temperatures reached +45.7 °C, also being the highest recorded temperatures since 1948. According to the Geographical Tables of Poland [33], Poland faced one of the biggest September heat waves on record in the second week of the month, with temperatures reaching +31 °C.

The goals of this paper are to demonstrate the capability of a developed-in-house algorithm to provide high temporal and spatial resolution SEVIRI AOD maps over Poland in near real-time, as well as to demonstrate the capacity of using the Raman Lidar derived AOD for validation purposes of satellite derived AOD, to compare the SEVIRI AOD with the AOD obtained with other measurements and model outputs, and finally to draw conclusions on any mutual effects of heat wave conditions on local and long-range transported air pollution and biomass burning smoke over Poland.

The paper is divided into various sections. In Section 2, the AOD retrieval schemes applied to the SEVIRI sensor and the Raman Lidar are introduced. In Section 3, the analyses of the heat wave event in the context of the changing optical properties of the atmosphere are given, whereby the observational ground-based data (PolandAOD, AERONET, EARLINET), satellite data (SEVIRI, MODIS) and model data (HYSPLIT, CAMS, NAAPS, GEM-AQ) are utilized. In Section 4, the paper is concluded. Note that all the abbreviations used above are explained and cited as they appear in the text and are acknowledged.

## 2. Methodology

### 2.1. Retrieval of Optical Properties from Raman Lidar Data

The automated 24/7 Lidar observations were conducted in the city-centre of Warsaw (52.21°N, 20.98°E, 112 m a.s.l.) at the Radiative Transfer Laboratory (RT-Lab) of the Institute of Geophysics, Faculty of Physics at University of Warsaw. The 12-channel NeXT Generation PollyXT Lidar [34] comprises a single laser as a light source for two optoelectronic detection units. The laser pulses (180 mJ at 1064 nm, 110 mJ at 532 nm and 60 mJ at 355 nm) are emitted into the atmosphere with a repetition rate of 20 Hz. Three laser beams are sent simultaneously and co-axially into the atmosphere (the initial laser beam is expanded to decrease beam divergence to 0.2 mrad). The backward scattered laser light is collected with large, narrow field of view (300 mm, 1 mrad) and small, wide field of view (50 mm, 2 mrad) Newtonian telescopes. The far-range detection unit uses an optical wavelength separator to determine the elastic scattering at 1064, 532 and 355 nm, as well as the elastic cross-polarized scattering at 532 and 355 nm, the vibrational Raman scattering for N<sub>2</sub> at 607 and 387 nm and for H<sub>2</sub>O at 407 nm. The near-range detection unit measures backward scattering at 532 and 355 nm (elastic), 607 and 387 nm (Raman) and is implemented to enhance the lowermost range of Lidar observations in a way

that allows its easy dismounting and usability with other Lidars. An incomplete geometrical overlap range between the emitted laser beam and the full field of view of the Lidar telescope affects the measured Lidar signals in the range close to the instrument. After the optical wavelength separators, the overlap range can be different at each channel. For data discussed here, the difference is negligible (at maximum  $\pm 15$  m for non-smoothed profiles) and all signals below 400 m altitude are regarded as overlap-range affected and rejected from further evaluation.

As a standard, the Lidar profiles are evaluated using the developed-in-house data processing chain (version VerlaufNG7.vi) written in LabView software environment (National Instruments: Austin, TX, USA). Details on evaluation schemes can be found in [35] (aerosol optical properties) and [25] (water vapor). The quality assurance and quality check procedures developed in the frame of the European Aerosol Research Lidar Network (EARLINET) are applied on a regular basis [36]. The daytime aerosol extinction backscattering coefficients and particle depolarization ratios are derived with the finest resolution of 20 min and 7.5 m (smoothing with running mean centered around 81st range bin is applied on the raw signals prior to the optical quantity retrieval). The water vapor profiles are derived at nighttime with the finest resolution of 30 min and 7.5 m; during daytime, the background skylight limits the detection capacity at 407 nm [25]. The aerosol extinction and backscatter coefficient profiles are derived by application of a classical Raman retrieval to the nitrogen channels at 387 and 607 nm, whereby the profiles of far-range and near-range detection are calculated separately from each other, and the far-near range merging is done on the profiles of physical quantities rather than on the arbitrary signals. The far-range backscatter profile is calibrated in an aerosol/cloud free range of the high troposphere and the near-range backscatter profile is merged with it by calibration with the far-range backscatter values obtained in the lower free troposphere at 3.5–4 km. In general, only a slight underestimation (below 5%) in the lowermost range (400–700 m) of the far-range backscatter is discerned; thus, often no merging is considered necessary for aerosol backscatter coefficient profiling. In contrast, the near-far range merging applied to the extinction profiles at a range where both profiles have the same extinction coefficient value within the uncertainty range for at least 300 m allows for the significant improvement of the aerosol extinction coefficient detection range down to  $450 \text{ m} \pm 30 \text{ m}$ . The Rayleigh molecular calibration is performed with the use of the atmospheric pressure  $p$  (hPa) and temperature  $T$  ( $^{\circ}\text{C}$ ) profiles obtained by RS92 radiosonde (Vaisala, Helsinki, Finland) launched with 12 h frequency at the closest World Meteorological Organization WMO-12374 station to Warsaw (about 25 km to the North-East) in Legionowo ( $52.40^{\circ}\text{N}$ ,  $20.96^{\circ}\text{E}$ , 96 m a.s.l.). Data sets are obtained via the Upper Air Data website ([weather.uwyo.edu/upperair/sounding.html](http://weather.uwyo.edu/upperair/sounding.html)) of the University of Wyoming. The surface temperature and pressure are taken from the WXT510 meteorological station (Vaisala, Helsinki, Finland) on the roof-platform of the RT-Lab (21 m a.g.l.) to reflect the local conditions directly at the Lidar site.

For calculation of the daytime aerosol optical depth (AOD), derived by Raman method, aerosol extinction coefficient profiles at 355 nm and 532 nm are linearly interpolated between the lowermost extinction value (available within the signal range not affected by the overlap) and the ground, using information at the surface. In the upper range, the interpolation of aerosol extinction profiles with exponential function shape is performed using the aerosol extinction value derived at 2.5–3.5 km (altitude limit assessed from the signal-to-noise ratio of each Raman channel) relative to the theoretical value of the Rayleigh molecular extinction at the tropopause level arbitrarily chosen at 15 km, where no load aerosol can be assumed. The Lidar-derived AOD columnar values were calculated by integrating the entire interpolated aerosol extinction coefficient profile (0–15 km). Additionally, the boundary layer height was derived dynamically for each profile as in [37,38]. The AOD was then calculated within the boundary layer range and in the free troposphere with a purpose to discern the local aerosol contribution from the aerosol related to a long-range transport of air masses.

## 2.2. Observations of Aerosols with Ceilometers

Aerosol structures were measured using CHM15k ceilometers (JenOptik/G. Lufft Mess- und Regeltechnik, Fellbach, Germany) at the Poland AOD sites in Strzyzow (SolarAOT Observatory) and Raciborz (Polish Academy of Sciences Observatory). The CHM15k instrument operates at single-wavelength of invisible 1064 nm laser radiation with 7–9  $\mu\text{J}$  pulse energy, 5–7 kHz pulse repetition rate and 1–5 ns pulse duration. The laser beam divergence is very small ( $<0.3$  mrad), and the output beam diameter is expanded to 90 mm. Only an elastic signal is detected in a photon counting mode. Typical averaging of the signals is over 15 min for a height resolution of 30 m. The receiver field of view is 45 mrad. The overlap of the receiver and emitter geometry is completed at circa 500 m. Data are stored in Network Common Data Form (NetCDF) files. The instrument targets the measurements of the aerosols, cloud droplets and ice crystals. The measured parameters are among others: raw backscatter data, cloud base height up to 9 layers (incl. penetration depth), sky condition and cloud amount.

## 2.3. Measurements of Aerosol Optical Depth Using Radiometers

Automatic sun-and-sky scanning photometers CE318 (CIMEL Electronique, Paris, France) were used to measure direct and diffuse solar irradiance and sky radiance at the Earth's surface at nine wavelengths (340, 380, 440, 500, 675, 870, 936, 1020, and 1640 nm), where the 936 nm channel is used to estimate the total water vapor column and the other channels are used for retrieval of AOD. Measurements are performed at the Polish Aerosol Research Network (PolandAOD) sites in Strzyzow (SolarAOT Observatory), Rzecin (PolWET Station of Poznan University of Life Sciences), Belsk and Raciborz (Polish Academy of Sciences Observatory). The datasets of raw measurements are uploaded and processed by the Aerosol Robotic NETwork (AERONET, [39]) to retrieve among others, spectrally dependent AOD with uncertainty at the level of  $\pm 0.01$  and total water vapor content.

Multifilter Rotating Shadowband Radiometers MFR-7 (Yankee Environmental Systems, Turners Falls, MA, USA) are used for continuous measurements of spectrally dependent AOD at three measurement sites of the PolandAOD network in Warsaw (RT-Lab of University of Warsaw), Strzyzow (SolarAOT Observatory) and Sopot (Polish Academy of Sciences Observatory). The instrument operates at six narrow-band channels (415, 500, 610, 675, 870 and 940 nm) and one broadband channel to measure direct, diffuse and total solar radiation. The instruments are regularly calibrated in situ using the classical Langley method. Due to the significant degradation of diffuser and filter optical properties that influence the channel sensitivity, the uncertainty of the retrieved MFR-7 AOD is higher than that of the CE318 instruments being at the level of  $\pm 0.025$ .

## 2.4. Retrieval of SEVIRI Aerosol Optical Depth

The Meteosat Second Generation (MSG) geostationary platform, developed by the European Organization for the Exploitation of Meteorological Satellites (EUMETSAT) in collaboration with the European Space Agency (ESA), is equipped with the Spinning Enhanced Visible and Infrared Imager (SEVIRI) instrument that provides observations of the Earth every 15 min, since 2004 [40]. The SEVIRI collects data in 12 spectral channels (in a range of 635 nm to 13.4  $\mu\text{m}$ ) with spatial resolution for a sub-satellite point of 3 km for channels 1–11 and 1 km in channel 12 (High Resolution Visible channel). Several approaches to the SEVIRI AOD daytime and night-time retrieval have been reported (e.g., [28–30]). In this paper we use the prototype version of the SEVIRI AOD algorithm developed in-house [28] that has been modified to provide AOD retrieval in near real-time over the territory of Poland. The algorithm is fed with the high temporal and spatial resolution radiance measurements from the SEVIRI visible channel 1 (635 nm) and allows for deriving AOD at 635 nm, at a spatial resolution of about  $5.5 \times 5.5 \text{ km}^2$  (due to the scan geometry for the area of Poland), at a frequency of 15 min.

The most important parameter for the AOD retrieval process is the assessment of the surface reflectance. The surface properties are estimated for particular conditions: during relatively cloud-free reference days (cloud cover over Poland < 0.6) which exhibit a low AOD (<0.15 at 550 nm), based on top-of-atmosphere (TOA) reflectance measured by the SEVIRI detector. However, even for low AODs, the elimination of influence of atmospheric components (in particular atmospheric aerosols) on the reflectance measured by satellite is still essential, thus several approaches to tackle this topic were proposed (e.g., [41,42]). In the algorithm used here, instead of the golden section search method and parabolic interpolation, an approach based on applying the optimal interpolation method [43] is used with the additional ground based sources of AOD data, that allow a reduction of the typical uncertainties related to the aerosol background estimation, and hence improve the AOD SEVIRI retrieval. A detailed description of the algorithm and uncertainty estimation was presented in [28].

The main changes introduced in the modified algorithm (apart from the main goal of optimizing it to derive near real-time SEVIRI AOD maps) are focused on including additional information for a background reference day, whereby choice strongly determines the uncertainty of the retrieval, as well as an application of an improved scheme for the cloud screening. In the new algorithm, instead of the Moderate Resolution Imaging Spectroradiometer (MODIS) AOD product, the Copernicus Atmosphere Monitoring Service (CAMS) AOD forecast data (<http://atmosphere.copernicus.eu>) are used as the input AOD background information [44,45]. Moreover, the data from all Polish ground-based sites of the Polish aerosol research network (PolandAOD website; [www.polandaod.pl](http://www.polandaod.pl)) that provide continuous AOD measurements in Sopot, Rzecin, Warsaw, Belsk, Raciborz, and Strzyzow are implemented in the modified code.

### 3. Results and Discussion

The Geographical Tables of Poland [33] indicate that September 2016 was extremely warm with a monthly anomaly of +2.57 °C, as calculated in relation to the average period of 1961–1990 (+2.36 °C for 1981–2010; +2.13 °C for 1991–2015). During the daytime, the September temperatures reached as high as +31 °C in the shade, and the night-time temperature drop was very low, down to exceptionally high values of 16–19 °C. By comparison, the Polish absolute temperature record was reported as +40.2 °C (in shadow) on 29 July 1921. According to the Synoptic Weather Charts Archive at the IMGW Website ([www.pogodynka.pl/polska/mapa\\_synoptyczna](http://www.pogodynka.pl/polska/mapa_synoptyczna)) [46], one of the biggest September heat waves on record was faced at the end of the first half of the month, spreading mainly over western and southern Poland. It then became cooler, but high temperatures were still observed until the end of the month. Therefore, to analyse the event, we focus on the crucial period of 11–16 September 2016.

The near-surface temperature and relative humidity measurements recorded by the WXT510 Vaisala meteorological station at Warsaw and Strzyzow sites ([www.poland.aod.pl](http://www.poland.aod.pl)) confirm the occurrence of the heat wave. At both measurement sites, the temperature and relative humidity are inversely proportional. They exhibit a daytime cycle with lower temperatures at night, and higher temperatures during the day, which are accompanied by an opposite cycle of the relative humidity. During the course of this event in Warsaw, the maximum temperature was obtained during the daytime with the highest values of 30–31 °C on 10 and 11 September, gradually dropping down to 25 °C on 16 September. The daytime relative humidity was very low, with minimal values between 29% and 35%. In general, the maximal surface temperature obtained in Strzyzow was lower, being 3 °C, and relative humidity was higher, being up to 12%. The observed temperature ranges indicate a heat wave occurrence as it is in opposition to typical thermal conditions trends for Poland [47].

According to the USA National Weather Service—National Oceanic and Atmospheric Administration (NOAA), the so-called heat index (HI) is defined as a measure of how hot it feels when relative humidity is factored with the apparent air temperature. The Heat Index Chart ([http://www.nws.noaa.gov/om/heat/heat\\_index.shtml](http://www.nws.noaa.gov/om/heat/heat_index.shtml)) relates the heat index value to the level of safety alert: HI of 26.7 °C to 32.2 °C caution level (fatigue for prolonged sun exposure and/or physical activity, to 38.9 °C extreme caution (possible sun-stroke, muscle cramps and heat exhaustion, to 52.2 °C danger (likely sun-stroke,

heat cramps, heat exhaustion and possible heat-stroke) and  $>52.2$  °C extreme danger (heat-stroke likely). The heat index values are defined for shady, light wind conditions and thus an exposure to full sunshine can increase the heat index values by up to 10 °C. On 8–13 September 2017, based on the meteorological measurements obtained in Warsaw, the heat index indicated values reaching 27.2 °C to 30.6 °C, which are labeled as caution level. On 14 September, the atmosphere started to cool down to reach a lower index value of 22.2 °C by 15 September, as related to long-range transport of cool and cleaner Arctic air mass. It then increased to 24.4 °C on 16 September, due to the influence of continental air from Eastern Europe.

The back-trajectories calculated using the HYSPLIT model [48,49] at 12:00 of Universal Coordinated Time (UTC) on each day of the event for 4 locations in Poland are given in Figure 1. Four sites of the PolandAOD network were chosen: Sopot (in the north of Poland, semi-urban site at the Baltic Sea coast), Rzecin (west-central Poland, wetland site, rural conditions), Warsaw (central Poland, urban site) and Strzyzow (in the south-east, a background mountain site). On each day, the backward-trajectories indicated different possible air mass transport. At most of the stations on 11–13 September, the air was advected from over East and South Germany, Czech Republic and Southern Scandinavia, but at Strzyzow, the air mass indicated fast transport from over Ukraine and Belarus. On 14 September, air was transported to all sites from over the Scandinavian and Baltic countries. On 15 September at all sites, the Arctic air masses were uniformly transported from over Northern Europe. On 16 September, air masses had a similar pathway only for the northernmost site in Sopot, for the trajectories which remained over South-Eastern Europe.

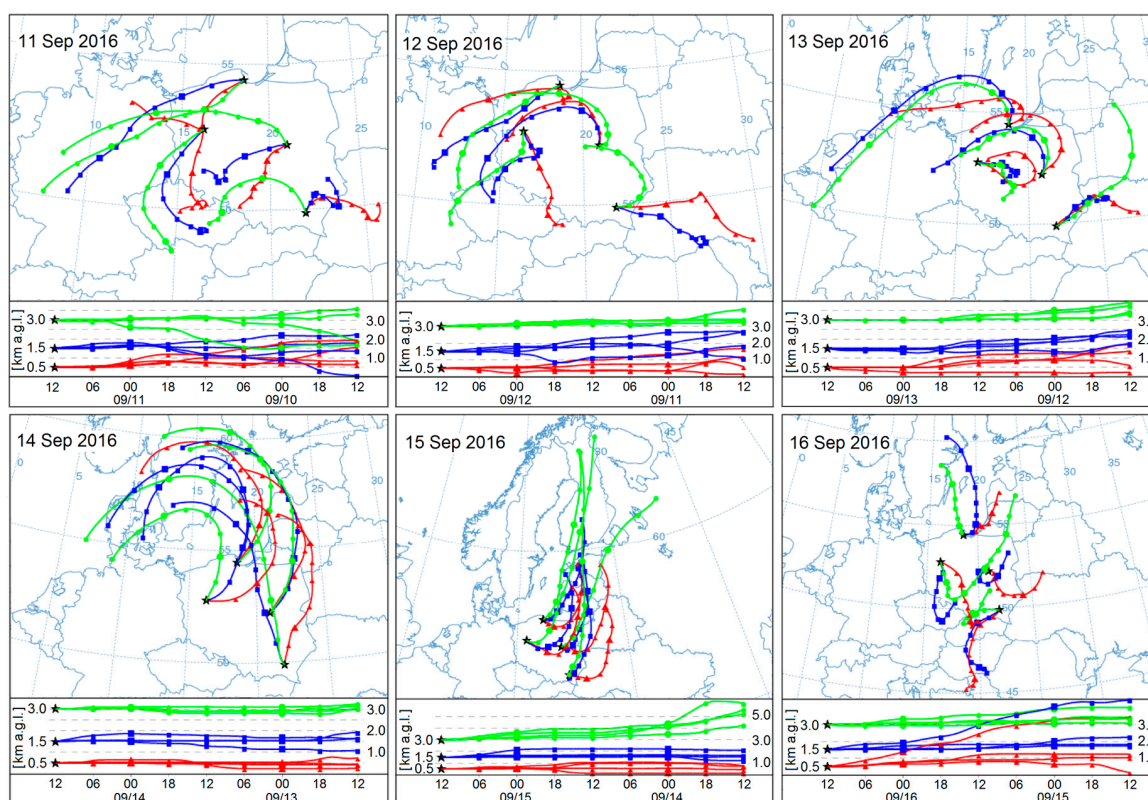


**Figure 1.** The NOAA HYSPLIT backward-trajectories obtained for the Poland AOD observational sites located in Sopot (northernmost), Rzecin (central-west), Warsaw (central-east), and Strzyzow (southernmost), arriving at those multiple locations at 12:00 UTC for 11–16 September 2016 (consecutive days are following in rows from the top-left). The model was run for 48 h, with meteorological data from the Global Data Assimilation System (GDAS).

### 3.1. Optical Properties with Ground-Based Active Remote Sensing

Ground-based, active remote measurements were available at three Poland AOD sites in Warsaw (central Poland), Strzyzow (south-eastern Poland, a vicinity on the Polish-Ukrainian border), and Raciborz (south-western Poland, a vicinity of the coal industry region of Silesia Region). In Warsaw, Lidar measurements with PollyXT Lidar were taken (shown in Figure 2). Observations with CHM15K ceilometers were performed in Strzyzow (Figure 3) and Raciborz (Figure 4). For all sub-plots, in each figure, the same colour scale was kept.

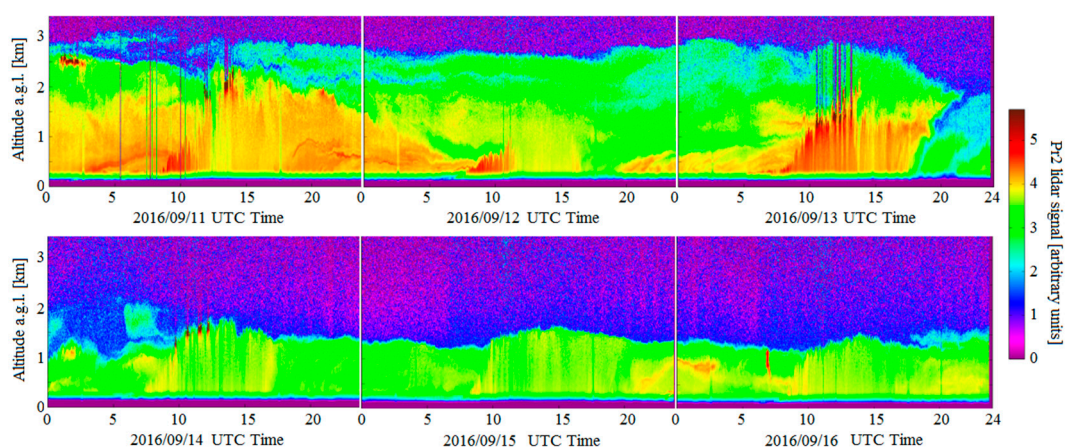


**Figure 2.** Range and background corrected signal at 1064 nm on 11–16 September 2016 during 24/7 measurements taken with the PollyXT Lidar in Warsaw (central Poland), (source: PolandAOD, [www.polandaod.pl](http://www.polandaod.pl)). Clearly visible atmospheric structures attributed to the anthropogenic pollution with much layering, increased aerosol load and an exceptionally highly elevated boundary layer (up to 3.2 km) due to the heat wave influence on 11–13 September. Thereafter, a clearing of the atmosphere occurred due to Arctic air mass intrusion and a decrease of the boundary layer (at 1.5 km) on 14 and 15 September and a rather typical aerosol scene for the Warsaw site on 16 September.

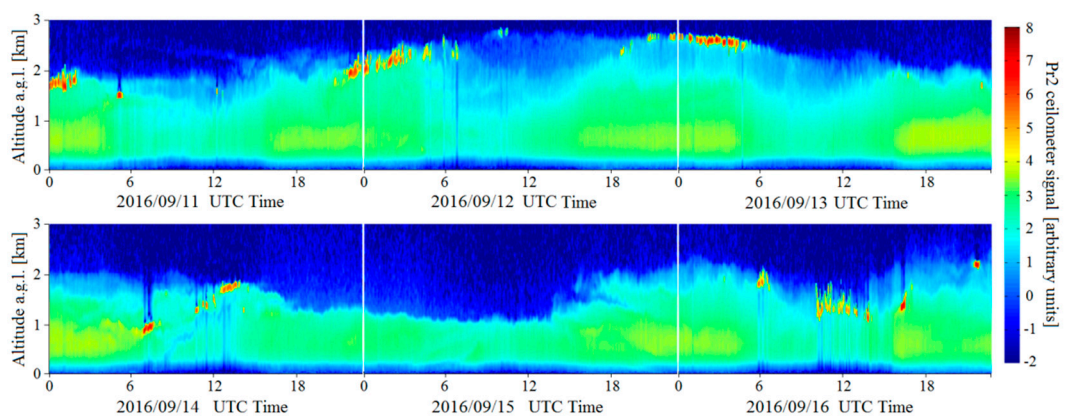


**Figure 3.** Range-corrected signal at 1064 nm of CHM15K ceilometer measurements taken in Strzyzow (south-eastern Poland); daylight effect in the ceilometer signal is manifested from 5:00 to 16:00 UTC (source: PolandAOD, [www.polandaod.pl](http://www.polandaod.pl)). The elevated boundary layer up to 2.2 km can be attributed to the transport of biomass-burning aerosol from Ukraine that was influenced by the heat wave on 12 and 13 September (further elevating boundary layer up to 2.7 km) and the aerosol removal due to Arctic air intrusion on 15 September (lowering boundary layer to 1.2 km).

In Warsaw, on 11–13 September, a distinctly high aerosol load can be discerned from 24/7 evolution plots of the 1064 nm Lidar signal. These are days with a well-increased aerosol load and possible occurrence (even accumulation) of transported and local pollution, compared with trajectories

in Figure 1. The boundary layer is very high, reaching up to 3.2 km a.g.l. (even for night-time residual layer), with distinct structures within. During the night in central Europe, a strong convection is not expected. A typical night time boundary layer height over Warsaw in September is <1.5 km and at daytime, the boundary layer top can reach approximately 2.8 km if strong convection and/or heat island effect occurs [37]. The extraordinarily strong elevation of boundary layer is likely due the heat wave. On 11 and 13 September, there is evidence of passing cumulus forming over the transition zone at around 12–14 UTC. On the next three days, 14–16 September, the boundary layer is much lower at 1.5–2 km a.g.l. (these values are more typical for summertime than autumn [37]), with still well distinguished morning transition, but not as much layering and structures as on 11–13 September.

At the Strzyzow site, the situation is different. On all days, the aerosol loads discerned from 24/7 evolution plots of the 1064 nm ceilometer signal, show accumulation of the aerosol in the lowermost 2–2.6 km a.g.l. (there is fair cloudiness indication in some profiles). Except for the period between 19:00 UTC on 19 September and 14:00 UTC on 15 September, where clearly, boundary layer height drops down to 1.25 km a.g.l., this drop, as at the Warsaw site, is likely related to the Arctic air mass inflow (compare Figure 1). However, the remaining aerosol structures seen in Strzyzow are likely to have originated from smoke and biomass burning aerosol transport, as indicated by the HYSPLIT backward trajectories (Figure 1). Indeed, the MODIS Global Fire Map 10-days composite, available for the period of 7–16 September 2016 (<https://lance.modaps.eosdis.nasa.gov/cgi-bin/imagery/firemaps.cgi>), confirmed the likeliness of a wild fire event of forest, peatland and/or grass burning over Ukraine.

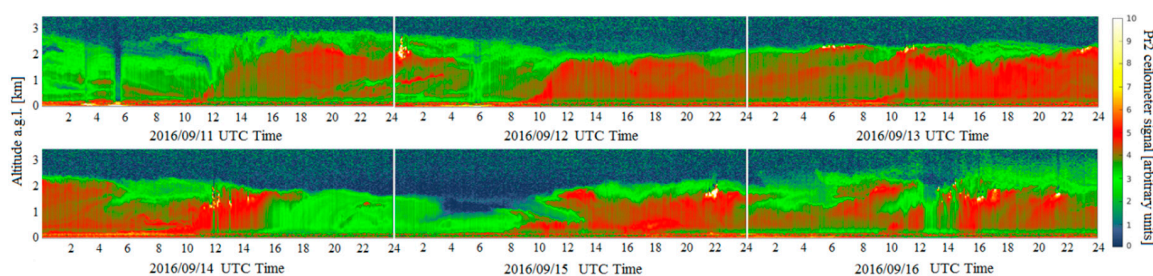


**Figure 4.** Range-corrected signal at 1064 nm of CHM15K ceilometer measurements taken in Raciborz (south-western Poland), (source: IGF-PAN [http://atmo.igf.edu.pl/Nimbus\\_Raciborz.php](http://atmo.igf.edu.pl/Nimbus_Raciborz.php)). The elevated boundary layer (2.2–2.9 km) attributed to both the anthropogenic pollution spread from Eastern Germany and the advection of biomass-burning aerosol from Ukraine, as influenced by a heat wave on 11–14 September; Arctic air intrusion at night of 14/15 September resulting in lowering of aerosol load and boundary layer to 1 km, after which the biomass burning aerosol dominated the scene.

As for the Raciborz site, the ceilometer signals (Figure 4) indicate similarities to the Warsaw site for 11–13 September (although the heat wave driven boundary layer is slightly lower at 2.2–2.9 km a.g.l.). There were even more similarities to the Strzyzow site for 14–16 September, with Arctic air-cleaning intrusion reaching the site at night on 14/15 September. Indeed, backward trajectories (Figure 1) indicate likely transport and mixing of polluted air mass from Germany and biomass burning particles from Ukraine over the Raciborz site.

### 3.2. Aerosol Properties from Model Output Simulation

The results of the Navy Aerosol Analysis and Prediction System—NAAPS model [50] simulations (<http://www.nrlmry.navy.mil/aerosol>) providing maps of AOD, sulphates, smoke and dust for Europe are given in Figure 5. A clear peak-patch of sulphate concentrations (16–32  $\mu\text{g}/\text{m}^3$ ) in Germany (in the Region of Saxony and on the west side of the borders with the Poland and Czech Republic) is seen for all days but 15 September. This peak-patch was accompanied by enhanced AODs (up to 1.6) only on 11–13 September, whereby AODs ‘drifted’ from Germany towards western Poland. Over Poland, the high AODs (up to 1.6) remained in the north-west and the sulphates were a significant part of

the aerosol load, reaching concentrations in a range of 2–16  $\mu\text{g}/\text{m}^3$ . In addition, smoke intrusions were indicated over south-eastern Poland (up to 16  $\mu\text{g}/\text{m}^3$ ). The period of 14–16 September was characterized by cleaner conditions with AOD in the range of 0.1–0.2 and sulphates reaching up to 16  $\mu\text{g}/\text{m}^3$  only over south-western Poland. The rest of the country's AODs were below 0.1 and sulphate concentrations below 8  $\mu\text{g}/\text{m}^3$  were forecast. Within the entire period, minimum values of AOD and sulphates are related to the atmosphere's cleaning due to the Arctic air mass inflow on 15 September. As for the smoke, a tendency to spread over southern and towards central Poland is discernible. Due to the location of the Strzyzow site in the south-east of Poland, there is a clear indication of relatively high smoke concentration (2–8  $\mu\text{g}/\text{m}^3$ ) during the entire period of 11–16 September 2016. Throughout the entire event, there was no indication of possible dust intrusions. In general, the NAAPS AOD seems to underestimate, with respect to all AOD data obtained for this period with ground-based and satellite instruments.

The Copernicus Atmosphere Monitoring Service—CAMS model [44,45] forecast of the AOD at 550 nm over Poland for the period of 11 to 16 September 2016 is plotted in Figure 6. The CAMS AOD maps reflect qualitative similarities with the NAAPS AOD maps. Here too, 11–13 September is indicated as having a higher aerosol load (AOD values of up to 0.5 in the northern part of Poland). The atmosphere begins to clear in the north-east of Poland and shifts the aerosol towards south-west on 14 September (values of 0.2–0.35). Finally, on 15 and 16 September, CAMS output indicates much cleaner conditions for the entire country with AODs of about 0.1.

**Table 1.** Aerosol optical depth (AOD) at 7:00, 8:00, 9:00 UTC (daily means are given in <>), particulate matter concentrations of a size of less than 2.5  $\mu\text{m}$  (PM<sub>2.5</sub>  $\mu\text{m}$ ), and Ångström exponent derived from various instruments over Warsaw on 11–16 September 2016.

| Instrument   | 11 September 2017 | 12 September 2017 | 13 September 2017 | 14 September 2017 | 16 September 2017 |
|--|-------------------|-------------------|-------------------|-------------------|-------------------|
| SEVIRI AOD at 635 nm                                   | 0.39              | 0.26              | 0.29              | 0.13              | 0.16              |
|  | 0.36              | 0.25              | 0.29              | 0.13              | 0.16              |
|  | 0.33              | 0.23              | 0.27              | 0.18              | 0.18              |
|  | <0.36>            | <0.25>            | <0.28>            | <0.15>            | <0.17>            |
|  |                   |                   |                   |                   |                   |
| MFR7 AOD at 675 nm                                     | 0.39              | 0.23              | 0.28              | 0.09              | 0.11              |
|  | 0.39              | 0.25              | 0.30              | 0.10              | 0.10              |
|  | 0.38              | 0.25              | 0.28              | 0.10              | 0.10              |
|  | <0.39>            | <0.24>            | <0.29>            | <0.1>             | <0.11>            |
|  |                   |                   |                   |                   |                   |
| Raman Lidar AOD at 532 nm                              | 0.27              | 0.23              | 0.22              | 0.11              | 0.13              |
|  | 0.33              | 0.22              | 0.23              | 0.12              | 0.16              |
|  | 0.32              | 0.20              | 0.21              | 0.16              | 0.19              |
|  | <0.31>            | <0.22>            | <0.22>            | <0.13>            | <0.16>            |
|  |                   |                   |                   |                   |                   |
| Raman Lidar AOD at 355 nm                              | 0.38              | 0.37              | 0.35              | 0.30              | 0.37              |
|  | 0.41              | 0.35              | 0.36              | 0.29              | 0.34              |
|  | 0.40              | 0.33              | 0.35              | 0.31              | 0.36              |
|  | <0.38>            | <0.35>            | <0.35>            | <0.30>            | <0.36>            |
|  |                   |                   |                   |                   |                   |
| SEVIRI PM <sub>2.5</sub> ( $\mu\text{g}/\text{m}^3$ )  | 33.65             | 25.27             | 28.95             | 9.73              | 17.65             |
| Surface PM <sub>2.5</sub> ( $\mu\text{g}/\text{m}^3$ ) | 28.8              | 22.3              | 19.6              | 8.6               | 16.8              |
| Ångström exponent (532/355)                            | 0.62              | 1.17              | 1.19              | 2.12              | 2.03              |

The Global Environmental Multiscale—Air Quality GEM-AQ model [51], forecast of the diurnal evolution of the aerosol extinction coefficient profiles for the locations of four sites: Sopot, Rzecin, Warsaw, and Strzyzow for 11–16 September 2016 is shown in Figure 7. The results for the whole period are in qualitative accordance with the NAAPS and the CAMS simulations; the lowest values are obtained at all sites for 15 September 2016. There are also high similarities of the GEM-AQ model extinction profiles evolution and the ceilometer signal plots in Strzyzow (Figure 3) and Raciborz (Figure 4), as well as with the Lidar signal plots in Warsaw (Figure 2). The similarity here is especially remarkable. Moreover, the values of the daytime AODs obtained in the boundary layer by integrating the model (500 nm) and Lidar (355 nm, 532 nm) aerosol extinction profiles (15 cases, Table 1) show a similar trend for all days of the event, except for 11 September, (where the GEM-AQ simulated lower

values), including AOD obtained by passive sensors, showing strong similarities of trend with AOD of GEM-AQ, can be reported for these four sites.

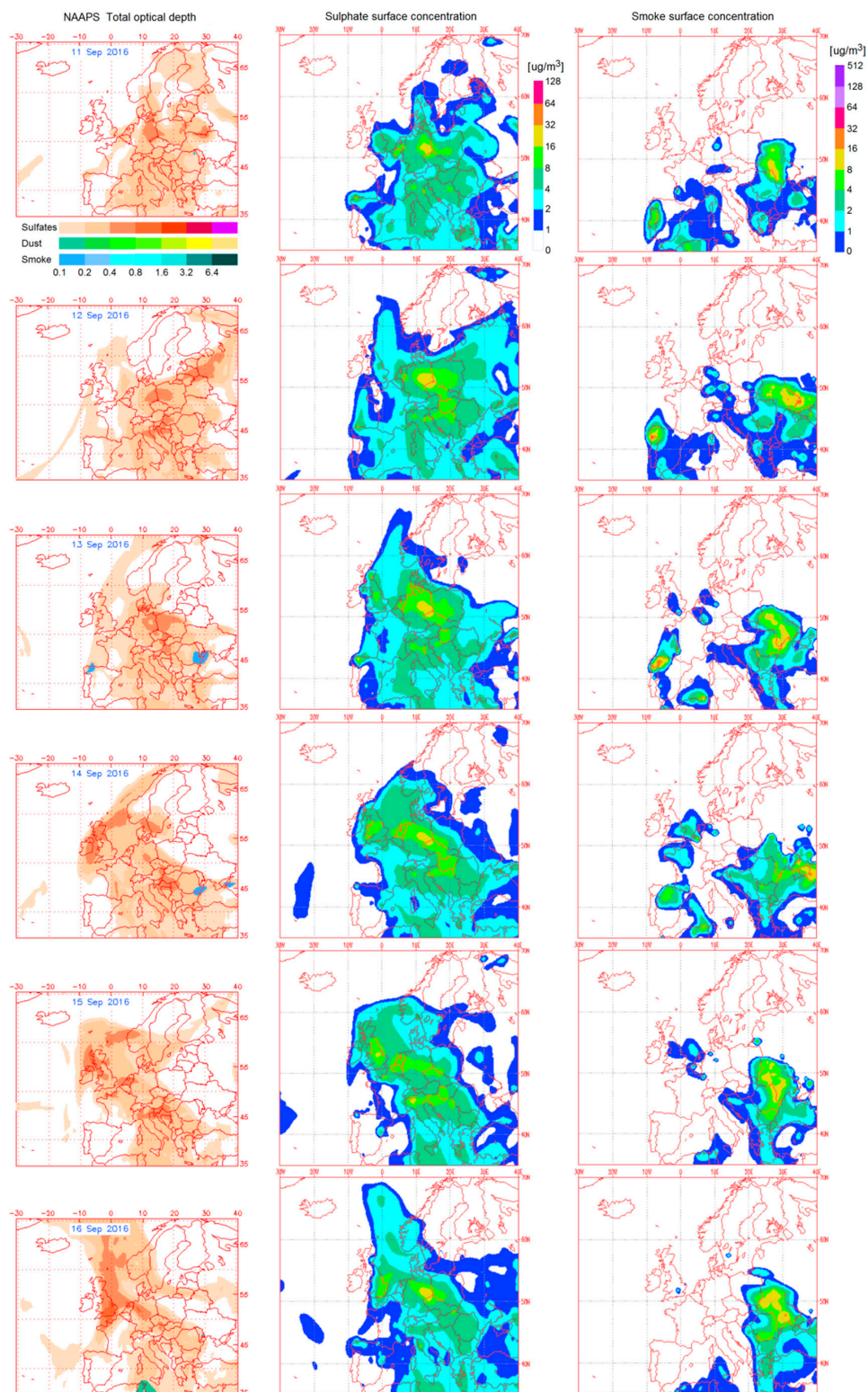


**Figure 5.** Aerosol optical depth (left) and concentration of sulphate surface (middle) and smoke (right) on 11–16 September 2016, obtained from Navy Aerosol Analysis and Prediction System (source: NAAPS, <http://www.nrlmry.navy.mil/aerosol>).

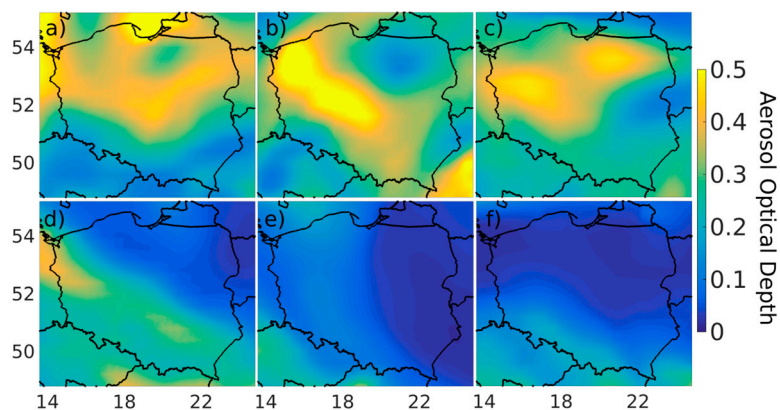


**Figure 6.** Aerosol optical depth at 550 nm forecast by CAMS at 6:00 UTC on 11–16 September 2016 ((a–f) indicate the consecutive days of the event), from upper left following rows (data source: <http://atmosphere.copernicus.eu>).

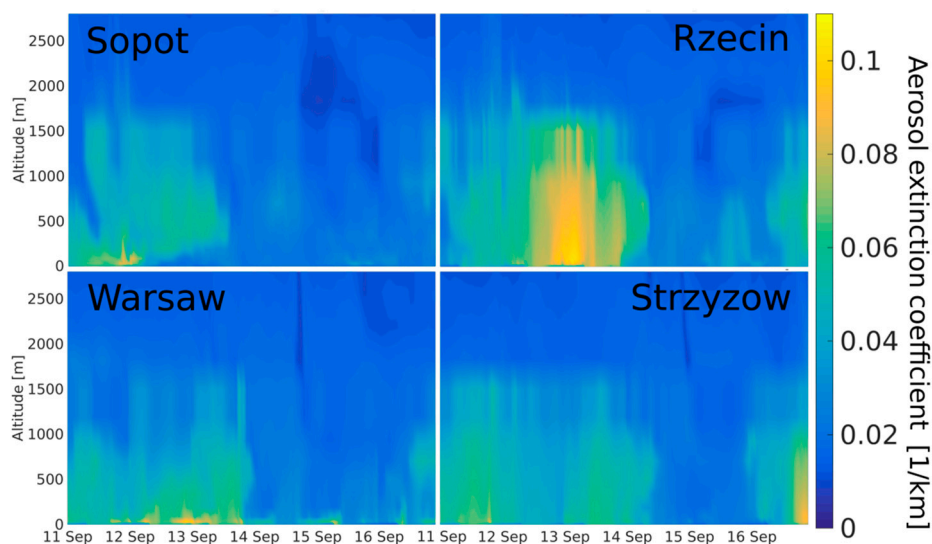


**Figure 7.** Aerosol extinction coefficient at 500 nm forecast by GEM-AQ model for Sopot, Rzecin, Warsaw, Strzyzow for 11–16 September 2016, (source: PolandAOD, [www.polandaod.pl](http://www.polandaod.pl)).

### 3.3. Optical Properties from Ground-Based Passive Remote Sensors

In fact, the discussed AOD (respective pixels) of NAAPS and CAMS, as well as GEM-AQ simulations, are in general accordance with the AOD data measured at the ground by the means of photometry and radiometry, as given in Figure 8. The hourly mean values of AOD were recorded at 5 locations of the PolandAOD network for the period of 11–16 September 2016. The Strzyzow, Rzecin, and Raciborz collected the AOD data with the CE318 photometer and the Sopot and Warsaw stations collected the AOD data with the MFR-7 radiometer. Temporal evolution of the AOD shown in Figure 8 indicates that the aerosol rich atmosphere had already cleared first in Sopot (the northernmost location) by 13 September, in central Poland (Warsaw and Rzecin) only a day later on 14 September and in the south at Strzyzow and Raciborz only on 15 September. On 16 September in Warsaw and Sopot, the conditions were similar; however, at the other three sites, the AOD had increased, which can be attributed to wild fire smoke aerosol transport in the South-East and/or pollution advection in the West.

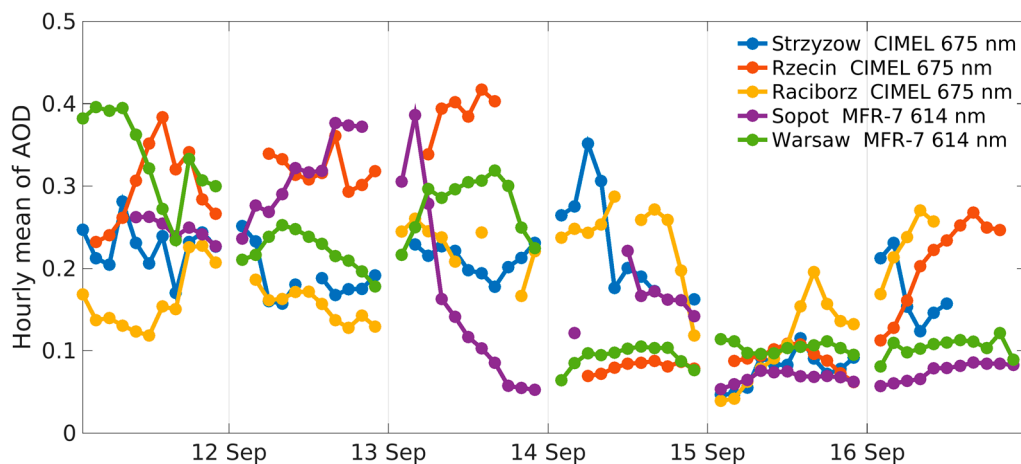


**Figure 8.** Aerosol optical depth (hourly mean) obtained at 5 sites of the PolandAOD network for the period 11–16 September 2016. At AERONET sites in Strzyzow, Rzecin, and Raciborz, AOD at 675 nm was measured using a CE318 photometer. At Sopot and Warsaw sites, AOD at 615 nm was derived from MFR-7 radiometer measurements at 614 nm.

The spectral dependence of the AOD for period 11–16 September 2016 at the Poland AOD sites in Rzecin, Raciborz, Strzyzow and Warsaw is depicted in Figure 9. In general, 15 September was distinguishably clearer at all sites (Figure 9, in green). In Warsaw there is a discernible separation in the spectral plots for 11–13 September (high load) and 14–16 September (lower load). The steep exponential-like shape of the spectra for the higher load period indicates an occurrence of small particles (of an approximate size of 400 nm). For the lower load, a similar abundance of small and larger particles occurred (size range of 400–900 nm). Over other sites, this high aerosol load of small size particles dominated, especially over Rzecin (the west-central location); on 12 and 13 September, values of AOD at 350 nm reached 0.85, clearly indicating anthropogenic pollution. In Rzecin, as in Warsaw, the atmosphere cleared on 14 and 15 September, but on 16 September increased again. In Raciborz (the west-south site) the situation is slightly different. The steep AOD spectra are present for all days, except for 15 September. On 11 and 12 September, AOD at 350 nm reaches 0.4–0.5 and on 12, 13 and 16 September, it increases to 0.7, whereby the spectra do not steepen, but are lifted, indicating an increase in aerosol load which may likely be due to smoke aerosol contribution. For Strzyzow again, 15 September AOD spectra are the lowest, and as for the rest, it is not feasible to unambiguously separate them.

For the three sites of Warsaw, Strzyzow and Raciborz, the ground-based active sensors measured the aerosol structures within the boundary layer and radiometers measured the corresponding columnar AOD. An increase of the boundary layer height due to heat trapped near the ground by the heat wave's stationary conditions can be related to the AOD measured by the radiometers.

For the Warsaw site, NAAPS indicated increased AODs due to a sulphate patch originating in Eastern Germany spreading towards central Poland (Figure 5). Thus, at this site only anthropogenic pollution is expected. A strong increase in the boundary layer due to the heat wave that manifested on 11–13 September (Figure 2) is well correlated with an increasing aerosol load and AOD (Figure 9). There is also a clear daytime AOD variation (Figure 8), capturing AOD increase and decrease, following the cycle of the Sun's elevation-angle change; although at night, due to Arctic air inflow on 13/14 September, the boundary layer is abruptly lowered from approximately 3 to 1.2 km a.g.l. and AOD at 675 nm from  $0.35 \pm 0.025$  to  $0.12 \pm 0.025$ . The relation of AOD and solar operation is weak but still discernible. Almost no differences in boundary layer height during day and night time for the entire period can be attributed to the heat wave driven lack of typical strong cooling at night, favouring rather strong residual layer formation and hindering nocturnal layer formation. Therefore, no significant differences between day and night AOD are expected.

At the Strzyzow site, NAAPS indicated low sulphates and strong smoke sources over Ukraine advancing towards southern Poland (Figure 5). Thus, at this site only biomass burning is expected. The increase of the boundary layer due to a heat wave is less intensive and occurs only on 12 and 13 September (Figure 3). It is anti-correlated with AOD (Figure 9) and slightly decreases with an increase of the boundary layer. There is no daytime AOD variation (Figure 8) with the Sun's operation. At night, due to Arctic-air intrusion on 14/15 September, the boundary layer lowers to circa 1.2 km a.g.l. (as at the Warsaw site), but AOD at 614 nm lowers from 2.5 to 0.05. Over the Raciborz site, NAAPS show an influence of high sulphates advancing from Germany and smoke from Ukraine (Figure 5), both increasing in intensity with time. The boundary layer increase due to a heat wave is less intensive than for Warsaw (up to 2.2–2.9 km a.g.l.), but persists for a longer time period on 11–14 September (Figure 4). There is no daytime AOD variation with the Sun's operation. Finding clear correlations of heat wave conditions with AOD is challenging. As expected from NAAPS, AOD at 614 nm slowly increased on each consecutive day from 0.12 to 0.28, until the Arctic air advection at night, of 14/15 September, when the boundary layer dropped to about 1.2 km a.g.l. and AOD drastically lowered ( $0.05 \pm 0.01$ ), similar to that of Strzyzow. On 16 September the AOD and boundary layer increased, mainly due to biomass burning aerosol advection.

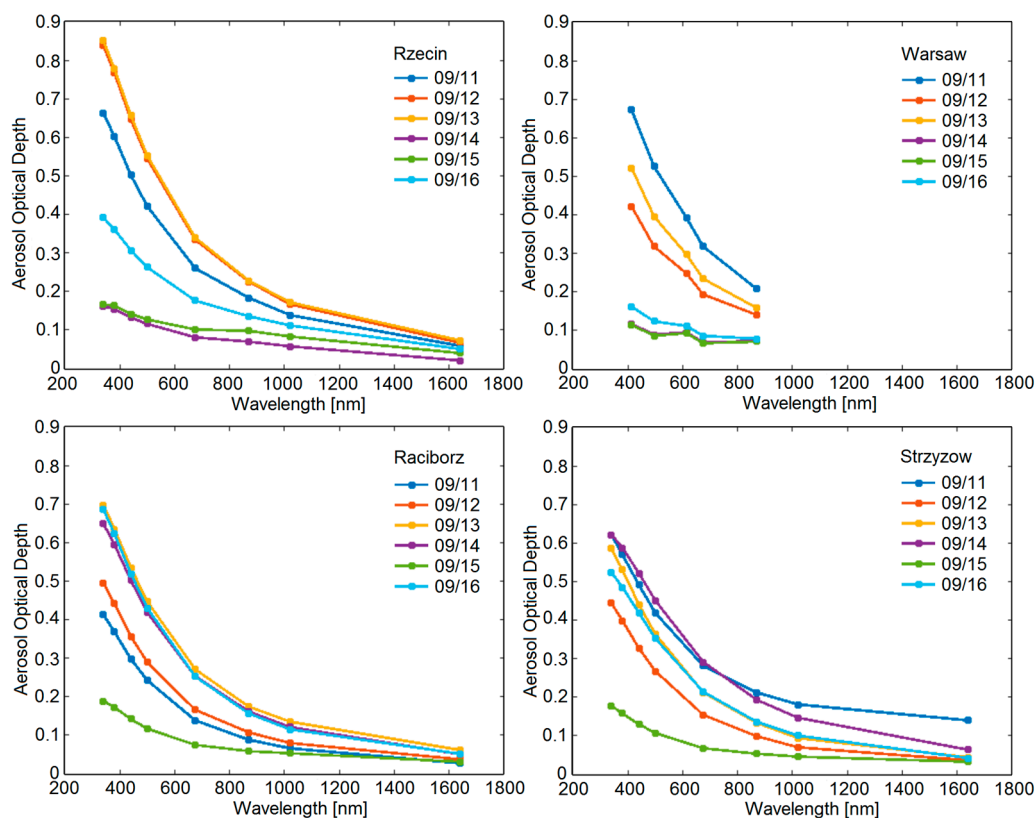


**Figure 9.** Spectral dependence of aerosol optical depth for the period 11–16 September 2016 at the Poland AOD sites in Rzecin (**top-left**), Warsaw (**top-right**), Raciborz (**bottom-left**), and Strzyzow (**bottom-right**). For each day, we selected the time point for which the ground-based AOD data and the SEVIRI AOD showed the highest agreement. For 15 September (the reference day), for all stations, the time point of 8:00 UTC was chosen.

### 3.4. Satellite-derived Aerosol Optical Depth Maps of Poland

For the derivation of the AOD maps over Poland for 11–16 September 2016, we used the new version of the SEVIRI AOD algorithm. Based on the AOD measurements at the five Poland AOD sites (Sopot, Rzecin, Raciborz, Strzyzow and Warsaw), 15 September 2016 was chosen as a reference day

for estimating the surface properties. On each day (except on the reference day), the daytime maps of AOD at 635 nm were calculated with a fine temporal resolution of 15 min from 5:30 till 9:00 UTC (14 maps/day). Within the selected time period, the SEVIRI AOD maps (in total 70; not shown here for brevity) visually revealed a low variability of AOD at such a high resolution. Thus in Figure 10, only the maps derived for each day at 7:00, 8:00 and 9:00 UTC are depicted. Indeed, for each day in Figure 10, the aerosol variability obtained at each consecutive hour does not vary much. The data indicated that the highest aerosol load over Poland (AOD > 0.3) was observed on 11–13 September. The strongest spatial variability of AOD was captured on 14 September, where a sharp edge of AOD stretched approximately 100 km off and along the western and southern borders of Poland, which can be attributed to the dynamic air-clearing process (fast transport of the Arctic air-mass had already begun). The lack of data in northern and western areas of the map (white pixels) is due to cloud cover. The SEVIRI AOD maps in Figure 10 well resemble the CAMS AOD maps in Figure 6, except for the 16 September, where CAMS clearly underestimates the AOD values and spatial variability.

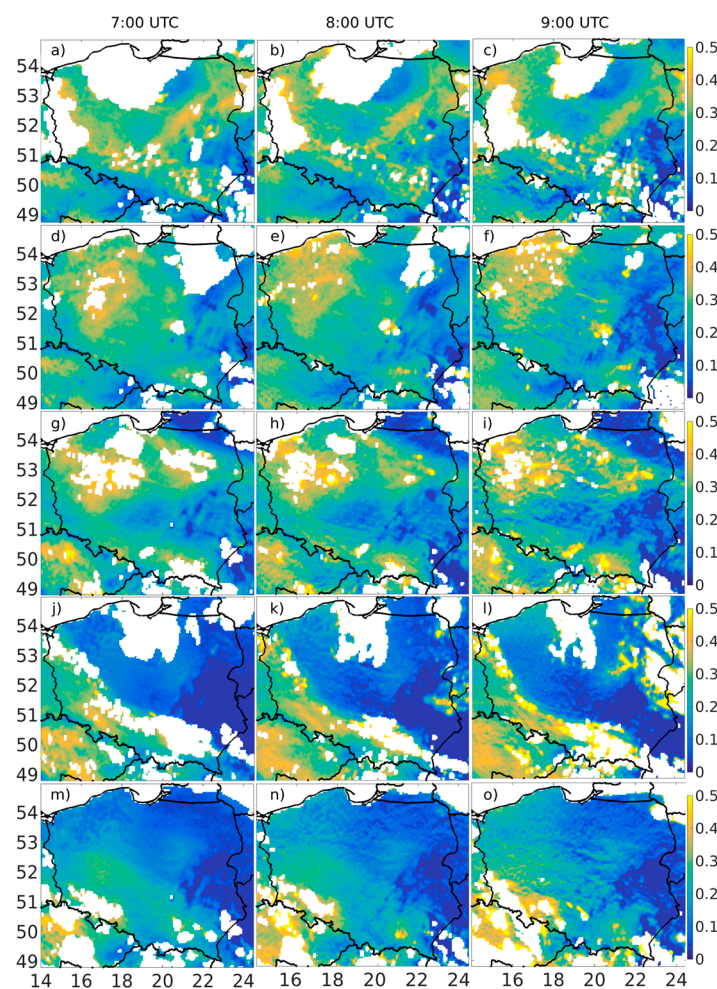


**Figure 10.** Aerosol optical depth obtained from SEVIRI sensor at 635 nm, calculated for 15 min at 7:00, 8:00, and 9:00 UTC on 11 (a–c), 12 (d–f), 13 (g–i), 14 (j–l) and 16 September 2016 (m–o), respectively. There is no retrieval on 15 September 2016 used as a reference day.

The validation of the new version of SEVIRI AOD algorithm was done by comparing the obtained SEVIRI AOD values, regarded as representative for the Warsaw pixel, with the AOD values obtained from the PollyXT Lidar profiles (Table 1) for 11–16 September 2016 (no reference day is included). During selected times, no clouds above Warsaw were observed by Lidar, except for 14 and 16 September, where some signatures of high level Cirrus clouds were captured. For further comparison, the Lidar

AOD at 532 nm (VIS) and 355 nm (UV) was scaled to 635 nm, using the power law with Ångström exponent value derived at the two wavelengths. In all cases (15 values), the scaled Lidar derived AODs at 635 nm are higher for VIS and slightly lower for UV, than the SEVIRI AOD for Warsaw pixel (Figure 11). The overestimation of the SEVIRI AOD is unlikely and caused by simple scaling of Lidar 355 nm AOD to 635 nm AOD for a large difference of the wavelengths (280 nm). The obtained good-agreement of the AOD Lidar and SEVIRI data (high correlation  $r^2$  of 0.86 for 355 nm and 0.85 for 532 nm) can be explained by the specifics of both retrieval algorithms. Firstly, for the Lidar AOD algorithm, the near-range detection unit allows for the extension of the Lidar aerosol extinction coefficient profiles down to approximately 400 m with respect to the far-range unit, that typically provides such profiles only down to about 1000 m. Secondly, the uncertainty of the Lidar-derived AOD and the SEVIRI-derived AOD decreases with the increasing aerosol load, unlike the MODIS AOD retrieval, where the uncertainty of AOD derivation is directly proportional to the aerosol load sensed [31,32]. The high aerosol loads observed during the studied heat wave event resulted in a good-agreement of the Lidar and SEVIRI AOD (Figure 11). In fact, an agreement of the obtained SEVIRI AOD at 635 nm maps with the MODIS AOD at 550 nm maps is reasonable (MODIS available only for 12, 13 and 15 September via [www.polandaod.pl](http://www.polandaod.pl); not shown for brevity); however, it is rather general, as the MODIS AOD maps are daily composites and are not directly comparable with the high temporal resolution of the derived SEVIRI AOD maps.

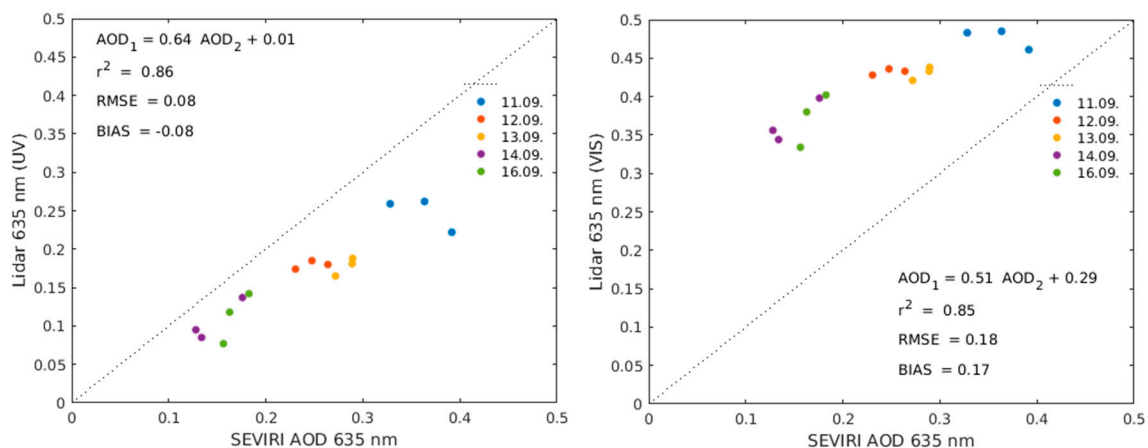


**Figure 11.** Comparison of the SEVIRI AOD pixel for Warsaw with the AOD derived from PollyXT Lidar in Warsaw on 11–16 September 2016. The aerosol optical depth was initially derived from Lidar daytime extinction profiles at 355 nm (UV; left sub-figure) and 532 nm (VIS; right sub-figure), and then scaled to the SEVIRI wavelength of 635 nm using the power law formula with Ångström exponent calculated individually for each data point.

The SEVIRI AOD was also validated by using the AOD data sets measured at the PolandAOD sites, which operate the AERONET (at 614 nm) photometers in Strzyzow, Rzecin, and Raciborz, or the MFR-7 (at 675 nm) radiometers in Warsaw, Strzyzow and Sopot. The correlation plots of the AOD measured at four of these sites with the SEVIRI AOD pixel for each site location are plotted for an observation period of 11–16 September 2016 in Figure 12 (no reference day is included). In general, the correlation is highest for Warsaw ( $r^2$  of 0.91) despite a large difference of the measured wavelength. It is also high for Raciborz (0.84) and for Rzecin (0.8), which is in agreement with correlations reported in literature [30]. For Warsaw and Raciborz clear separation of the data points is visible; however, different trends are discerned. In Figure 12, the upper right sub-figure for Warsaw, a gradual AOD decrease on each consecutive day of the event is visible (on 11 September of 0.35, 12 September 0.28, 13 September 0.22 and 14–16 September 0.14). In the bottom left sub-figure the opposite for Raciborz is observed, an increase from lower AOD values on 11 September (0.18) and 12 September (0.2) to 0.3 on the remaining days. For Rzecin and Strzyzow the separation is not as clear. As expected, a low

correlation and an overestimation of the SEVIRI AOD was obtained for the Strzyzow site ( $r^2$  of 0.57), which can be attributed to the high altitude elevation of this site, located at on the hill (444 m a.s.l.) and thus, a low representativeness of the large SEVIRI pixel for this site.

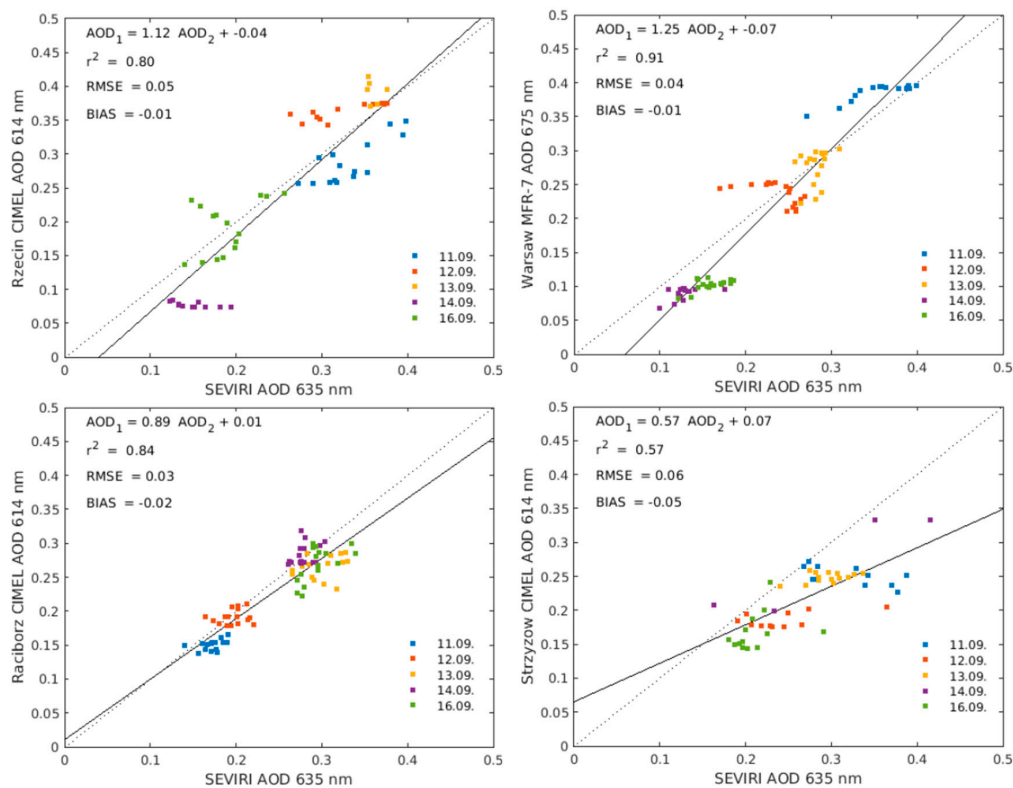


**Figure 12.** Correlation plot of the AOD measured at the Poland AOD sites in Rzecin (**top-left**), Warsaw (**top-right**), Raciborz (**bottom-left**) and Strzyzow (**bottom-right**), with the SEVIRI AOD pixel derived for these locations during the period of 11–16 September 2016.

The obtained SEVIRI AOD is slightly underestimated in comparison to the Lidar measurements and the radiometric observations. On the one hand, this can be attributed to the inaccurate estimation of the surface properties during the reference day (15 September). The Lidar measurements confirm that this day was not a clean one (aerosol signatures are not for a typical clean background in Warsaw). Although on that day, the maximum value of the Lidar aerosol extinction coefficient at 532 nm was nearly 10 times lower than the maximum value measured on 11 September. A closer look at the Lidar derived intensive and extensive properties, indicates an existence of small particles with Ångström exponent  $AE(532/355)$  strongly oscillating around 2 within the ground and 2.4 km. During 14 September, such low values were also obtained. This, accompanied with a very low linear polarization ratio of  $0.018 \pm 0.04$  at 532 nm, Lidar ratio of  $50 \pm 12$  sr at 532 nm, indicates that 15 September was typical for background conditions contaminated with slight anthropogenic pollution of urban origin.

On the other hand, one has to bear in mind that the SEVIRI AODs are not directly comparable with the AODs obtained from Lidar, nor from radiometric observations. First of all, the difference in the compared AOD wavelengths has to be taken into account (even if AODs are scaled to the SEVIRI wavelength). Secondly, ground-based measurements are representative for a single point, while the SEVIRI data cover an area of around  $5.5 \times 5.5$  km<sup>2</sup>, and thus the AOD is in fact a mean value for the whole pixel. Regarding inherent limitations of the least squares method itself, it always produces the result with the smallest sum of squares of errors, although there is no guarantee that this result has any physical meaning. In particular, if there are many outliers in the dataset, the results may have

nothing to do with the actual trend line or the relationship between the phenomena described by the random variables. The least squares method is adapted to the points furthest from the mean, which can introduce the greatest error. A single outlier that is very distant from the rest will force a trend line. As outliers may be common in real data, prior to the use of the least squares method, careful data checking for outliers (scatter plot) was performed. No outliers were found/removed in the analyzed data sets.

Finally, the SEVIRI AOD was converted to the particulate matter concentrations of a size of less than  $2.5 \mu\text{m}$  (the SEVIRI PM<sub>2.5</sub>) with a simple approach, by assuming that the daily mean of the SEVIRI AOD obtained by averaging all of the derived daytime AOD values for the Warsaw pixel, normalized to the value of the daytime AOD obtained by the ground-based Lidar in Warsaw (scaled to SEVIRI wavelength), shall be proportional to the daily PM<sub>2.5</sub> derived from the satellite data normalized to the daily PM<sub>2.5</sub> value at the surface. For normalization, the PollyXT AODs calculated from the ground level to the dynamically derived boundary layer and the surface daily mean PM<sub>2.5</sub> data of the Regional Inspectorate of Environmental Protection (WIOS) monitoring site in Warsaw-Ursynow (<http://sojp.wios.warszawa.pl/raport-dobowy-i-roczny>) were used. The obtained values of the SEVIRI PM<sub>2.5</sub> and the surface WIOS PM<sub>2.5</sub> at Warsaw-Ursynow site are given in Table 1, where as expected, the satellite derived values are higher than the values obtained at the surface. Since for the SEVIRI AOD normalization the Lidar-derived AODs were calculated within the boundary layer, the contribution of the free troposphere to the SEVIRI PM<sub>2.5</sub> can be assessed. It was in the order of 4.8 to 14.4% on all days of the event, with the exception of 13 September, when it increased to 22.9%. Hence, most of the aerosol load and particulate matter were confined to the boundary layer during the analyzed period. These results also indicate a good qualitative correspondence between the range-corrected attenuated backscatter Lidar signals (Figure 2) and the PM<sub>2.5</sub> concentration at the ground (Table 1), regardless of poor (PM<sub>2.5</sub> >  $30 \mu\text{g}/\text{m}^3$ ), moderate or high air-quality (PM<sub>2.5</sub> <  $10 \mu\text{g}/\text{m}^3$ ). The Lidar signals intensity increases with the increasing PM<sub>2.5</sub> concentration and/or decreases with an inflow of clean air masses to Warsaw. Moreover, both the daily mean of the SEVIRI PM<sub>2.5</sub> data at the Warsaw pixel, as well as the daily mean surface WIOS PM<sub>2.5</sub> data are anti-correlated with respect to the Ångström exponent (ÅE) obtained from the Lidar extinction profiles at 532 nm and 355 nm, as depicted in Figure 13 and Table 1, whereby the poor and moderate air-quality conditions observed on the first three days of the event revealed low and moderate values of ÅE. After the air cleaning related to the inflow of the Arctic air mass on 14 September, the decrease of the PM<sub>2.5</sub> values is accompanied with a significant ÅE increase, indicating occurrence of small size particles.

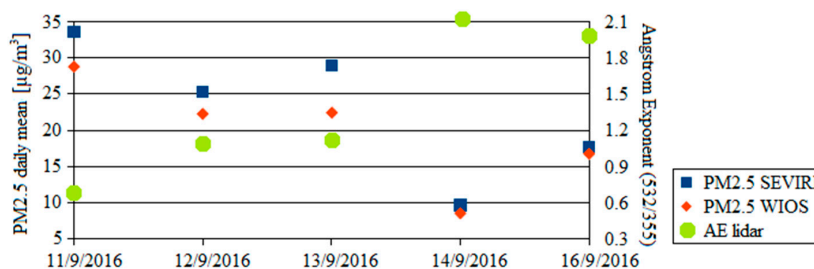


**Figure 13.** Daily mean values of the surface SEVIRI PM<sub>2.5</sub> for the Warsaw pixel (in blue) and the surface PM<sub>2.5</sub> measured at WIOS site in Warsaw Ursynow (in red), during the period of 11–16 September 2016. The PM<sub>2.5</sub> daily mean values are anti-correlated with the daily mean Ångström exponent obtained from the PollyXT Lidar extinction profiles in Warsaw.

#### 4. Conclusions

Particle optical properties, characteristic for aerosols that were suspended in the atmosphere during the heat wave event around 11–16 September 2016 over Poland, were analysed. To conclude on a horizontal extent of the event; geostationary SEVIRI-MSG sensor was exploited for quasi-continuous,

high temporal (15 min) and spatial ( $5.5 \times 5.5 \text{ km}^2$ ) resolution air quality monitoring. The optimal interpolation approach was used to derive SEVIRI AOD maps over Poland and it was validated with the ground-based and satellite AOD measurements and compared to model data.

The comparisons of SEVIRI AOD maps with the NAAPS and CAMS models AOD maps generally indicate a good qualitative agreement; however, model data are underestimated. On the other hand, the SEVIRI AOD (single location pixel) was found to be slightly underestimated in comparison to radiometric observations (columnar AOD), which can at least be partly attributed to the surface properties during the chosen reference day (15 September), having not been as clean as necessary or expected. Potential for validation of the SEVIRI AOD with the AOD derived from daytime Raman Lidar measurements (PollyXT in Warsaw), was successfully explored. Undoubtedly, a combination of near-far Lidar detection range for the aerosol extinction retrieval positively affected the Lidar AOD derivation. The Lidar AODs also indicated underestimation of SEVIRI AOD. Indeed, on the reference day chosen for SEVIRI retrieval, the Lidar measurements in Warsaw confirmed background conditions contaminated with slight urban pollution, what likely caused the underestimation. There are certainly inherent biases in relation to indirect measurements of the SEVIRI AOD. The AOD maps are derived by using information from the ground-based AODs and thus, the comparisons of SEVIRI AOD pixel with the ground-based AODs are biased (all radiometers), except for the comparison with the Lidar derived AODs.

The SEVIRI AOD converted to SEVIRI PM<sub>2.5</sub> (for the Warsaw pixel) remained higher than the surface PM<sub>2.5</sub>, as expected. The contribution of the free troposphere to the SEVIRI PM<sub>2.5</sub> was of 4.8 to 14.4% on all days of the event (except one day), indicating aerosol load and particulate matter strictly confined to the boundary layer during the heat wave. The surface daily mean PM<sub>2.5</sub> was anti-correlated with the Lidar derived mean daytime Ångström exponent. The highest PM<sub>2.5</sub> values observed reaching  $30 \mu\text{g}/\text{m}^3$  were related to relatively low values of ÅE (532/355) of  $0.7 \pm 0.2$ , and lowest PM<sub>2.5</sub> of  $10 \mu\text{g}/\text{m}^3$  was related to high values of ÅE of  $2 \pm 0.3$ .

According to the HYSPLIT backward-trajectories, detected aerosol structures and layers characterized by different optical properties also have a different origin: biomass burning aerosols from fires in Ukraine, anthropogenic pollution air-masses that a few days earlier had circulated over Eastern Germany and clean air-mass transported from the Arctic. For the observed event, there is clearly a heat wave relation to the pollution, which seems to be intensified in heat wave conditions, as well as to the long-range transport of biomass burning particles, which seem to be moderated by the heat wave. Over the urban site in Warsaw, dominated by anthropogenic pollutants (local and advected non-absorbing sulphates from Germany), a boundary layer increase due to the heat wave is significant (up to 100%) and is accompanied by an approximate linear increase of aerosol load and optical depth (10% increase of boundary layer height results in 8–12% increase of AOD). Contrarily, over the rural site in Strzyow, dominated by fresh biomass burning aerosol (composed of sulphate and absorbing soot particles transported from Ukraine), the heat wave driven boundary layer increase is less pronounced (up to 45%) and is related to aerosol optical depth decrease (10% increase of boundary layer height results in around 4% decrease of AOD). For a semi-urban site in Raciborz, it is difficult to discern clear relations of aerosol optical properties with the heat wave conditions, due to mixing of local and advected anthropogenic pollutants from Germany, with long-range transported aged biomass burning particles from Ukraine. However qualitatively, on the days during which pollution dominated over Raciborz, similar but less pronounced correlations as in Warsaw, were observed, and for the days dominated by biomass burning anti-correlations as in Strzyow. Regardless of the measurement site, the intrusion of the relatively clean Arctic air mass from the North of Europe resulted in washing off the aerosols, lowering the daytime boundary layer height to 1–1.2 km a.g.l. at all sites, and decreasing the aerosol optical depth to  $0.05 \pm 0.01$  at 614 nm in Strzyow and Raciborz (typical background aerosol values at these sites) and to  $0.12 \pm 0.025$  at 675 nm in Warsaw (slightly higher than the typical background).

**Acknowledgments:** We acknowledge Alison Smuts-Simons for the Scientific-English proof reading of this paper. The algorithm for the aerosol optical depth retrieval from the Meteosat Second Generation (MSG) Spinning Enhanced Visible and Infrared Imager (SEVIRI) was developed in the frame of the SAteellite based Monitoring Initiative for Regional Air quality (SAMIRA) project funded by the ESA-ESRIN Contract No. 4000117393/16/I-NB. The SEVIRI data were obtained from EUMETSAT, license No. 50001643. The algorithm for the aerosol optical depth retrieval from the Next Generation PollyXT Lidar was developed in the frame of the Technical assistance for Polish Radar and Lidar Mobile Observation System (POLIMOS) project funded by ESA-ESTEC Contract No. 4000119961/16/NL/FF/mg. The development of the PollyXT Lidar was financed by the Polish Foundation of Science and Technology (FNTP-No. 519/FNITP/115/2010) and the Polish National Science Centre (NCN-SONATABIS-2012/05/E/ST10/01578). Lidar was developed in a collaboration of scientists from the University of Warsaw and the Institute of Tropospheric Research (TROPOS) in the PollyXT development group of Dietrich Althausen. The RT-Lab located in the city center of Warsaw, central Poland, is a part of the Polish aerosol research network (PolandAOD, [www.polandaod.pl](http://www.polandaod.pl)). The station represents the only Polish Raman Lidar site within the European Aerosol Research Lidar Network (EARLINET, [www.earlinet.org](http://www.earlinet.org)) and the worldwide Polly.NET Lidar network ([www.polly.tropos.de](http://www.polly.tropos.de)). We acknowledge Aleksander Pietruczuk and Artur Szkop for the use of ceilometer data from the Polish Academy of Sciences Observatory in Raciborz ([http://atmo.igf.edu.pl/Nimbus\\_Raciborz.php](http://atmo.igf.edu.pl/Nimbus_Raciborz.php)). We acknowledge Brent Holben, Bogdan Chojnicki, Krzysztof Markowicz and Aleksander Pietruczuk for the use of data from the AERONET sites at Rzecin, Strzyzow, and Raciborz (<https://aeronet.gsfc.nasa.gov>). We acknowledge Krzysztof Markowicz for the use of the data collected at the Poland AOD website (PolandAOD, [www.polandaod.pl](http://www.polandaod.pl)). This paper contains modified Copernicus Atmosphere Monitoring Service Information (2017); neither the EC nor the ECMWF is responsible for any use that may be made of the information it contains. The (HYSPLIT) model was used via the Real-time environmental applications and display system (READY) website (<http://ready.arl.noaa.gov>) of the NOAA Air Resources Laboratory. The EARLINET is currently supported by the ACTRIS-2 project, funded by the European Union Research Infrastructure Action under the H2020 specific program for Integrating and opening existing national and regional research infrastructures of European interest under Grant Agreement No. 654109 (2015e2019). The University of Warsaw participates in ACTRIS-2 project as an associate partner without funding.

**Author Contributions:** Iwona S. Stachlewska wrote the paper, contributed to the design and building of the PollyXT Lidar, conducted Lidar observations, developed Lidar algorithms and performed Lidar retrieval, analyzed and interpreted all results. Olga Zawadzka developed the algorithm and performed SEVIRI AOD retrieval, validated it with passive ground-based sensors, prepared the majority of figures and conducted a merit revision of the manuscript. Ronny Engelmann contributed to PollyXT Lidar hardware and software design and development, and conducted a merit revision of the manuscript.

**Conflicts of Interest:** Authors declare no conflict of interest.

## References

- Bernstein, D.N.; Neelin, J.D.; Li, Q.B.; Chen, D. Could aerosol emissions be used for regional heat wave mitigation? *Atmos. Chem. Phys.* **2013**, *13*, 6373–6390. [[CrossRef](#)]
- Meehl, G.A.; Tebaldi, C. More intense, more frequent, and longer lasting heat waves in the 21st century. *Science* **2004**, *305*, 994–997. [[CrossRef](#)] [[PubMed](#)]
- Dalla-Marta, P.M.; Haylock, M.R.; Luterbacher, J.; Wanner, H. Doubled length of western European summer heat waves since 1880. *J. Geophys. Res.* **2007**, *112*, D15103. [[CrossRef](#)]
- Tomczyk, A.M.; Bednorz, E. Heat waves in Central Europe and their circulation conditions. *Int. J. Climatol.* **2016**, *36*, 770–782. [[CrossRef](#)]
- Lyamani, H.; Olmo, F.J.; Alcántara, A.; Alados-Arboledas, L. Atmospheric aerosols during the 2003 heat wave in southeastern Spain I: Spectral optical depth. *Atmos. Environ.* **2006**, *40*, 6453–6464. [[CrossRef](#)]
- Lyamani, H.; Olmo, F.J.; Alcántara, A.; Alados-Arboledas, L. Atmospheric aerosols during the 2003 heat wave in southeastern Spain II: Microphysical columnar properties and radiative forcing. *Atmos. Environ.* **2006**, *40*, 6465–6476. [[CrossRef](#)]
- Penner, J.E.; Dickinson, R.E.; O'Neill, C.A. Effects of aerosol from biomass burning on the global radiation budget. *Science* **1992**, *256*, 1432–1435. [[CrossRef](#)] [[PubMed](#)]
- Zhang, Q.; Ma, X.; Tie, X.; Huang, M.; Zhao, C. Vertical distributions of aerosols under different weather conditions: Analysis of in situ aircraft measurements in Beijing, China. *Atmos. Environ.* **2009**, *43*, 5526–5535. [[CrossRef](#)]
- Collaud, C.M.; Weingartner, E.; Furger, M.; Nyeki, S.; Prévôt, A.S.H.; Steinbacher, M.; Baltensperger, U. Aerosol climatology and planetary boundary influence at the Jungfraujoch analyzed by synoptic weather types. *Atmos. Chem. Phys.* **2011**, *11*, 5931–5944. [[CrossRef](#)]

10. Dörnbrack, A.; Stachlewska, I.S.; Ritter, C.; Neuber, R. Aerosol distribution around Svalbard during intense easterly winds. *Atmos. Chem. Phys.* **2010**, *10*, 1473–1490. [[CrossRef](#)]
11. Quan, J.; Gao, Y.; Zhang, Q.; Tie, X.; Cao, J.; Han, S.; Meng, J.; Chen, P.; Zhao, D. Evolution of planetary boundary layer under different weather conditions, and its impact on aerosol concentrations. *Particuology* **2013**, *11*, 34–40. [[CrossRef](#)]
12. Jacob, D.J.; Winner, D.A. Effect of climate change on air quality. *Atmos. Environ.* **2009**, *43*, 51–63. [[CrossRef](#)]
13. Wang, H.; Xue, M.; Zhang, X.Y.; Liu, H.L.; Zhou, C.H.; Tan, S.C.; Che, H.Z.; Chen, B.; Li, T. Mesoscale modeling study of the interactions between aerosols and PBL meteorology during a haze episode in Jing–Jin–Ji (China) and its nearby surrounding region—Part 1: Aerosol distributions and meteorological features. *Atmos. Chem. Phys.* **2015**, *15*, 3257–3275. [[CrossRef](#)]
14. European Union. *Air Quality in Europe—2016 Report*; European Environment Agency EEA Report No. 28/2016; Publications Office of the European Union: Luxembourg, 2016.
15. Katsouyanni, K.; Pantazopoulou, A.; Touloumi, G.; Tselepidaki, I.; Moustiris, K.; Asimakopoulos, D.; Pouloupoulou, G.; Trichopoulos, D. Evidence for interaction between air pollution and high temperature in the causation of excess mortality. *Arch. Environ. Health* **1993**, *48*, 235–242. [[CrossRef](#)] [[PubMed](#)]
16. Patz, J.A.; Campbell-Lendrum, D.; Holloway, T.; Foley, J.A. Impact of regional climate change on human health. *Nature* **2005**, *438*, 310–317. [[CrossRef](#)] [[PubMed](#)]
17. Fischer, P.H.; Brunekreef, B.; Lebre, E. Air pollution related deaths during the 2003 heat wave in the Netherlands. *Atmos. Environ.* **2004**, *38*, 1083–1085. [[CrossRef](#)]
18. Shaposhnikov, D.; Revich, B.; Bellander, T.; Bedada, G.B.; Bottai, M.; Kharkova, T.; Kvasha, E.; Lezina, E.; Lind, T.; Semutnikova, E.; et al. Mortality related to air pollution with the Moscow heat wave and wildfire of 2010. *Epidemiology* **2014**, *25*, 359–364. [[CrossRef](#)] [[PubMed](#)]
19. Janicka, L.; Stachlewska, I.S.; Veselovskii, I.; Baars, H. Temporal variations in optical and microphysical properties of mineral dust and biomass burning aerosol derived from daytime Raman Lidar observations over Warsaw, Poland. *Atmos. Environ.* **2017**, *169*, 162–174. [[CrossRef](#)]
20. Markowicz, K.M.; Chilinski, M.T.; Lisok, J.; Zawadzka, O.; Stachlewska, I.S.; Janicka, L.; Rozwadowska, A.; Makuch, P.; Pakszys, P.; Zielinski, T.; et al. Study of aerosol optical properties during long-range transport of biomass burning from Canada to Central Europe in July 2013. *J. Aerosol Sci.* **2016**, *101*, 156–173. [[CrossRef](#)]
21. Ortiz-Amezcu, P.; Guerrero-Rascado, L.L.; Granados-Muñoz, M.J.; Benavent-Oltra, J.A.; Böckmann, C.; Samaras, S.; Stachlewska, I.S.; Janicka, L.; Baars, H.; Böhlmann, S.; et al. Microphysical characterization of long-range transported biomass burning particles from North America at three EARLINET stations. *Atmos. Chem. Phys.* **2017**, *17*, 5931–5946. [[CrossRef](#)]
22. Pyta, H.; Rosik-Dulewska, C.; Czaplicka, M. Speciation of ambient mercury in the Upper Silesia Region, Poland. *Water Air Soil Pollut.* **2009**, *197*, 233–240. [[CrossRef](#)]
23. Pastuszka, J.S.; Rogula-Kozłowska, W.; Zajusz-Zubek, E. Characterization of PM<sub>10</sub> and PM<sub>2.5</sub> and associated heavy metals at the crossroads and urban background site in Zabrze, Upper Silesia, Poland, during the smog episodes. *Environ. Monit. Assess.* **2010**, *168*, 613–627. [[CrossRef](#)] [[PubMed](#)]
24. Maciszewska, A.E.; Markowicz, K.M.; Witek, M.L. A multiyear analysis of aerosol optical thickness over Europe and Central Poland using NAAPS model simulation. *Acta Geophys.* **2010**, *58*, 1147–1163. [[CrossRef](#)]
25. Stachlewska, I.S.; Costa-Sueros, M.; Althausen, D. Raman Lidar water vapor profiling over Warsaw, Poland. *Atmos. Res.* **2017**, *194*, 258–267. [[CrossRef](#)]
26. Taravat, A.; Proud, S.; Peronaci, S.; Del Frate, F.; Oppelt, N. Multilayer perceptron neural networks model for meteosat second generation SEVIRI daytime cloud masking. *Remote Sens.* **2015**, *7*, 1529–1539. [[CrossRef](#)]
27. Hammer, A.; Kühnert, J.; Weinreich, K.; Lorenz, E. Short-term forecasting of surface solar irradiance based on meteosat-SEVIRI data using a nighttime cloud index. *Remote Sens.* **2015**, *7*, 9070–9090. [[CrossRef](#)]
28. Zawadzka, O.; Markowicz, K.M. Retrieval of aerosol optical depth from optimal interpolation approach applied to SEVIRI data. *Remote Sens.* **2014**, *6*, 7182–7211. [[CrossRef](#)]
29. Gonzalez, L.; Briottet, X. North Africa and Saudi Arabia day/night sandstorm survey (NASCube). *Remote Sens.* **2017**, *9*, 896. [[CrossRef](#)]
30. Zhang, Y.; Li, Z.; Qie, L.; Hou, W.; Liu, Z.; Zhang, Y.; Xie, Y.; Chen, X.; Xu, H. Retrieval of aerosol optical depth using the empirical orthogonal functions (EOFs) based on PARASOL multi-angle intensity data. *Remote Sens.* **2017**, *9*, 578. [[CrossRef](#)]

31. Belle, J.H.; Liu, Y. Evaluation of aqua MODIS collection 6 AOD parameters for air quality research over the Continental United States. *Remote Sens.* **2016**, *8*, 815. [[CrossRef](#)]
32. Nichol, J.E.; Bilal, M. Validation of MODIS 3 km resolution aerosol optical depth retrievals over Asia. *Remote Sens.* **2016**, *8*, 328. [[CrossRef](#)]
33. Libner, P.; Stefaniak, G. *Tablice Geograficzne (The Geographical Tables of Poland)*; Kram: Warsaw, Poland, 2017.
34. Engelmann, R.; Kanitz, T.; Baars, H.; Heese, B.; Althausen, D.; Skupin, A.; Wandinger, U.; Komppula, M.; Stachlewska, I.S.; Amiridis, V.; et al. The automated multiwavelength Raman polarization and water vapor Lidar PollyXT: The neXT generation. *Atmos. Meas. Tech.* **2016**, *9*, 1767–1784. [[CrossRef](#)]
35. Baars, H.; Kanitz, T.; Engelmann, R.; Althausen, D.; Heese, B.; Komppula, M.; Preißler, J.; Tesche, M.; Ansmann, A.; Wandinger, U.; et al. An overview of the first decade of PollyNET: An emerging network of automated Raman-polarization Lidars for continuous aerosol profiling. *Atmos. Chem. Phys.* **2016**, *16*, 5111–5137. [[CrossRef](#)]
36. Pappalardo, G.; Amodeo, A.; Apituley, A.; Comeron, A.; Freudenthaler, V.; Linné, H.; Ansmann, A.; Bösenberg, J.; D'Amico, G.; Mattis, I.; et al. EARLINET towards an advanced sustainable European aerosol Lidar network. *Atmos. Meas. Tech.* **2014**, *7*, 2389–2409. [[CrossRef](#)]
37. Holben, B.N.; Eck, T.F.; Slutsker, I.; Tanré, D.; Buis, J.P.; Setzer, A.; Vermote, E.; Reagan, J.A.; Kaufman, Y.J.; Nakajima, T.; et al. AERONET—A federated instrument network and data archive for aerosol characterization. *Remote Sens. Environ.* **1998**, *66*, 1–16. [[CrossRef](#)]
38. Stachlewska, I.S.; Piadlowski, M.; Migacz, S.; Szkop, A.; Zielinska, A.J.; Swaczyna, P.L. Ceilometer observations of the boundary layer over Warsaw, Poland. *Acta Geophys.* **2012**, *60*, 1386–1412. [[CrossRef](#)]
39. Sokół, P.; Stachlewska, I.S.; Ungureanu, I.; Stefan, S. Evaluation of the boundary layer morning transition using the CL-31 ceilometer signals. *Acta Geophys.* **2014**, *62*, 367–380. [[CrossRef](#)]
40. Aminou, D.M. MSG's SEVIRI Instrument. *ESA Bull.* **2000**, *111*, 15–17.
41. Popp, C.; Hauser, A.; Foppa, N.; Wunderle, S. Remote sensing of aerosol optical depth over central Europe from MSG-SEVIRI data and accuracy assessment with ground-based AERONET measurements. *J. Geophys. Res.* **2007**, *112*, D24S11. [[CrossRef](#)]
42. Mei, L.; Xue, Y.; de Leeuw, G.; Holzer-Popp, T.; Guang, J.; Li, Y.; Yang, L.; Xu, X.; Li, C.; Wang, Y.; et al. Retrieval of aerosol optical depth over land based on a time series technique using MSG/SEVIRI data. *Atmos. Chem. Phys.* **2012**, *12*, 9167–9185. [[CrossRef](#)]
43. Rodgers, C. *Inverse Methods for Atmospheric Sounding: Theory and Practice*; Series on Atmospheric, Oceanic and Planetary Physics; World Scientific: Singapore, 2000; Volume 2.
44. Benedetti, A.; Morcrette, J.-J.; Boucher, O.; Dethof, A.; Engelen, R.J.; Fischer, M.; Flentjes, H.; Huneeus, N.; Jones, L.; Kaiser, J.W.; et al. The GEMS-AER team. Aerosol analysis and forecast in the ECMWF Integrated Forecast System. Part II: Data assimilation. *J. Geophys. Res.* **2009**, *114*, D13205. [[CrossRef](#)]
45. Morcrette, J.J.; Boucher, O.; Jones, L.; Salmond, D.; Bechtold, P.; Beljaars, A.; Benedetti, A.; Bonet, A.; Kaiser, J.W.; Razinger, M.; et al. Aerosol analysis and forecast in the ECMWF Integrated Forecast System. Part I: Forward modeling. *J. Geophys. Res.* **2009**, *114D*, D06206. [[CrossRef](#)]
46. IMGW. Available online: [www.pogodynka.pl/polska/mapa\\_synoptyczna](http://www.pogodynka.pl/polska/mapa_synoptyczna) (accessed on 22 November 2017).
47. Owczarek, M.; Filipiak, J. Contemporary changes of thermal conditions in Poland, 1951–2015. *Bull. Geogr.* **2016**, *10*, 31–50. [[CrossRef](#)]
48. Draxler, R.R.; Rolph, G.D. *HYSPLIT (HYbrid Single-Particle Lagrangian Integrated Trajectory)*; Model Access via NOAA ARL READY Website; NOAA Air Resources Laboratory: Silver Spring, MD, USA, 2010. Available online: <http://ready.arl.noaa.gov/HYSPLIT.php> (accessed on 8 October 2017).
49. Rolph, G.D. *Real-Time Environmental Applications and Display System (READY)*; NOAA Air Resources Laboratory: Silver Spring, MD, USA, 2016. Available online: <http://ready.arl.noaa.gov> (accessed on 8 October 2017).
50. Lynch, P.; Reid, J.S.; Westphal, D.L.; Zhang, J.; Hogan, T.F.; Hyer, E.J.; Curtis, C.A.; Hegg, D.A.; Shi, Y.; Campbell, J.R.; et al. An 11-year global gridded aerosol optical thickness reanalysis (v1.0) for atmospheric and climate sciences. *Geosci. Model Dev.* **2016**, *9*, 1489–1522. [[CrossRef](#)]
51. Kaminski, J.W.; Neary, L.; Struzewska, J.; McConnell, J.C.; Lupu, A.; Jarosz, J.; Toyota, K.; Gong, S.L.; Côté, J.; Liu, X.; et al. GEM-AQ, an on-line global multiscale chemical weather modeling system: Model description and evaluation of gas phase chemistry processes. *Atmos. Chem. Phys.* **2008**, *8*, 3255–3281. [[CrossRef](#)]



© 2017 by the authors. Licensee MDPI, Basel, Switzerland. This article is an open access article distributed under the terms and conditions of the Creative Commons Attribution (CC BY) license (<http://creativecommons.org/licenses/by/4.0/>).